Nonadiabatic Transition in the A-Band Photodissociation of Ethyl Iodide from 294 to 308 nm by Using Velocity Imaging Detection

Xiao-Peng Zhang, Wei-Bin Lee, and King-Chuen Lin*

Department of Chemistry, National Taiwan University, Taipei 106, and Institute of Atomic and Molecular Sciences, Academia Sinica, Taipei 106, Taiwan

Photodissociation dynamics of ethyl iodide in the A-band is investigated at wavelengths between 294 and 308 nm using resonance-enhanced multiphoton ionization technique combined with velocity imaging detection. The I/I* branching, translational energy disposals, anisotropy parameters, and curve crossing probabilities of the dissociation channels are determined. The $I(5p^2P_{3/2})$-product channel is found to have hotter internal states of C_2H_5, and the $I*(5p^2P_{1/2})$ channel is accompanied by colder C_2H_5. Anisotropy parameters (β) for the I* channel remain at 2.0, indicating that the I* production should originate from the $^3Q_0$ state. The β values are from 1.6 to 1.9 in the I-product channel, which comprises two components of direct excitation of $^3Q_1$ and nonadiabatic transition between the $^3Q_0$ and $^1Q_1$ states. The curve crossing probability rises rapidly around the conical intersection but remains almost constant after passing through the curve crossing. The $^1Q_1$ and $^3Q_0$ states in the exit region are thus expected to cross almost parallel along the dissociation coordinate. As compared to the case of CH_3I, the nonadiabatic transition probabilities are slightly enhanced by an ethyl-substituted group.

I. Introduction

Photochemistry of alkyl halides has received wide attention for decades, in part because of their importance to the environmental impact. Alkyl halides may undergo C−X (X = Cl, Br, I) bond fission, upon UV excitation to the A-band (n, σ*) that comprises three overlapping states denoted as $^3Q_1$, $^3Q_0$, and $^1Q_1$ in the ascending order by Mulliken.[1] The A-band photodissociation of CH_3I leads to CH_3 and spin−orbit ground $I(5p\ ^2P_{3/2})$ or spin−orbit excited $I*(5p\ ^2P_{1/2})$.[2−13] The $^3Q_0$ $(2A_1)$ state correlates to the I* fragment with a transition dipole moment aligned parallel to the C−I bond, whereas the $^3Q_1(2E)$ and $^1Q_1(3E)$ states correlate to I with the transition dipole moment perpendicular to the bond axis. I* was reported as the major product, and a small I product was attributed to a curve crossing from the $^3Q_0(2A_1)$ to $^1Q_1(3E)$ state. CH_3I may evolve to a C_s symmetry during dissociation, when a $H_3C−I$ bending mode is coupled to the dissociation axis.[14−16] The $^1Q_1(3E)$ state therefore splits into A′ and A″ states, and the coupling between the $^3Q_0(3A′)$ and $^1Q_1(4A′)$ states enhances the nonadiabatic transition. Such nonadiabatic nature of the multidimensional photodissociation has strong influence on the ultrafast reaction rates for each dissociation channel.[17] The resulting CH_3 moiety is thus complicated with various multimode excitation but dominated by the umbrella mode.[6]

As compared with methyl iodide, the photodissociation dynamics of C_2H_5I and other α-branched heavier alkyl iodides have been less studied. In general, these alkyl iodides dissociate as rapidly as CH_3I in the regime of 10−200 fs. Such an ultrafast dynamic behavior has been characterized in terms of resonance Raman or photoelectron spectra from the alkyl iodide cations as measured in gaseous vapors or nonpolar solvents.[6,18−20] Despite rapid dissociation, the α-branched alkyl iodides having lower molecular symmetry should cause difference in the

nonadiabatic transition. According to the one-dimensional Landau−Zener model, the heavier branches lead to a slower velocity through the curve crossing region such that the $^3Q_0$ state may have more probability to transit into the $^1Q_1$ state.[21] For instance, $\Phi(I*)$, a quantum yield of I*, for CH_3I was obtained as about 0.73 ± 0.04 in the wavelength range 248−266 nm, and then decreased to 0.13 ± 0.07 at 304 nm.[12,22] When a bulkier size is branched to the α-carbon atom, $\Phi(I*)$ was obtained to be 0.44 ± 0.03 and 0.20 ± 0.03 for isopropyl and isobutyl iodide, respectively, at 266 nm,[23] and 0.03 for *tert*-butyl iodide at 277 nm.[24] The α-bulky group enhances the strength of the $^3Q_0 \rightarrow ^1Q_1$ nonadiabatic transition and brings about the decrease of $\Phi(I*)$. Although a qualitative agreement is reached in their dynamic trend, controversy still exists in understanding the detailed complexity.[25,26]

As compared to CH_3I, the A-band absorption spectrum of C_2H_5I appears to slightly blue shift to a region of 200−310 nm, peaking at 258 nm.[27,28] Energy partitioning and I*/I branching have been the focus of the study.[21,25,29,30] The consequences rely on the excitation wavelength and the nonadiabatic nature of the A-band photodissociation. A recent study of the photodissociation of ethyl iodide over the wavelength range of 245−283 nm provided the quantum yields of I and I* as well as the related anisotropy parameters.[31] Accordingly, the curve crossing probabilities were determined to rise gradually with the wavelength. But the photolyzing wavelengths are away from the region of the conical intersection such that the behavior of the nonadiabatic transition can not be effectively compared with the case of CH_3I. By taking advantage of resonance-enhanced multiphoton ionization (REMPI) technique combined with velocity imaging detection, we extend the photolyzing wavelengths to 294−308 nm in this work, thereby looking into the influence of geometric difference on the photodissociation dynamics of C_2H_5I. The speed and angular distributions of I and I* are analyzed to determine the subsequent spatial anisotropies and the relative quantum yields at different pho-

tolyzing wavelengths. The curve crossing probabilities between the $^3Q_0$ and $^1Q_1$ states are then evaluated and compared to the case of methyl iodide to understand the ethyl-substituted effect.
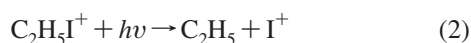
II. Experimental Section

The apparatus is similar to that used previously.[31−33] A <5% C_2H_5I sample (99% purity) was carried by helium gas at 1 atm through a pulsed valve with 0.6 mm diameter orifice (General Valve Co.), operating at 10 Hz and expanded into the source chamber. After passing through a 1 mm diameter skimmer and a collimator, the molecular beam was intersected perpendicularly by a linearly polarized laser beam in a two-stage ion lens region. The skimmer was mounted 30 mm downstream from the nozzle to divide the source chamber from the detection chamber.

A 308 nm excimer laser-pumped dye laser (FL3002, Lambda Physik) was frequency-doubled to emit the wavelengths from 294 to 308 nm with the energy 20−200 μJ, followed by linear polarization perpendicular to the flight tube direction, and then focused at the skimmed beam with a 200 mm focal-length lens. The laser pulses were focused to the leading edge of the molecular beam to minimize the cluster formation. The C_2H_5I molecules were then photolyzed and the subsequent I and I* fragments, as selectively ionized by a $(2 + 1)$ REMPI scheme, were velocity-mapped onto a two-stage microchannel plate (MCP) and a phosphor screen (FM3040, Galileo). The MCP could be gated within a minimum duration of 250 ns for mass selection. The ion imaging on the phosphor screen was recorded by a charge coupled device (CCD) camera (200XL4078, Pixelfly). The laser wavelength was scanned back and forth within the range of Doppler broadening to cover all the velocity components of the selected fragments. All the ion signals without the gate restriction may be transferred to a transient digitizer for display of the mass spectrum. The laser power dependence of the ion intensity was acquired directly from the transient digitizer.

III. Results and Discussion

A. I and I* Ion Images. The ion images of I and I* photofragments were acquired at four pairs of dissociation wavelengths, 294.1/298.2, 303.7/304.0, 304.7/305.6, 306.6/307.6 nm, beyond which no I/I* pairs can be probed significantly in the A-band absorption. Each raw image was accumulated over 40000 laser shots with the background removed and then restored to its Abel-inversed three-dimensional spatial distribution of the fragment. Examples of the raw and reconstructed ion images are given in Figures 1 and 2. The corresponding speed distributions of I* and I extracted from these ion images are also shown in the figures. Each of them can be well fitted by a narrow Gaussian curve, suggesting that I and I* are produced from direct dissociation along the repulsive potential energy surfaces after absorbing one UV photon.

The I$^+$ contribution alternatively by the dissociative ionization channels should be negligible. They may be expressed by

$$C_2H_5I + 2h\upsilon \rightarrow C_2H_5I^+ \qquad (1)$$

$$C_2H_5I^+ + h\upsilon \rightarrow C_2H_5 + I^+ \qquad (2)$$

$$C_2H_5I^+ \rightarrow C_2H_5{}^+ + I \qquad (3)$$

$$I + 3h\upsilon \rightarrow I^+ \qquad (4)$$

The channels via eqs 1 and 2 are blocked as a result of the wavelength larger than 266 nm. The details were discussed previously.[31] If the dissociative ionization channel proceeds
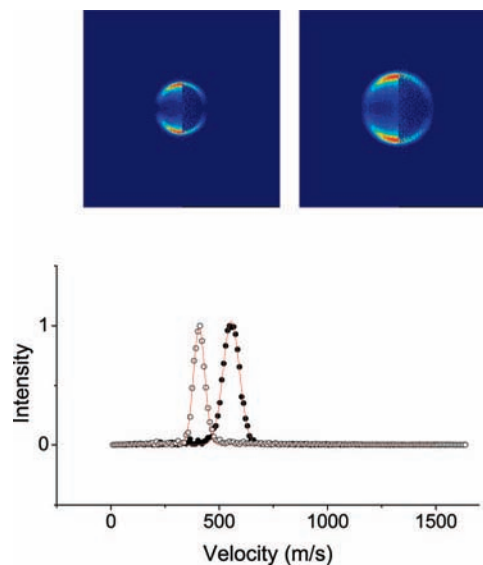
Figure 1. Ion images and speed distributions of I (right) and I* (left) from the photodissociation of C_2H_5I at 303.7 and 304.0 nm. The left half is the raw ion image, and the right half is the inverse Abel-transformed one. The laser beam is linearly polarized along the vertical direction. The normalized I and I* speed distributions are denoted by the closed-circle and open-circle data points, respectively. The Gaussian fits are denoted by the solid lines.
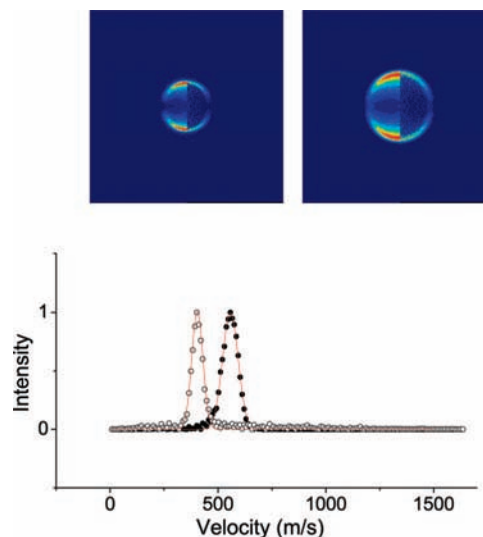
Figure 2. Ion images and speed distributions of I (right) and I* (left) from the photodissociation of C_2H_5I at 304.7 and 305.6 nm. The left half is the raw ion image, and the right half is the inverse Abel-transformed one. The laser beam is linearly polarized along the vertical direction. The normalized I and I* speed distributions are denoted by the closed-circle and open-circle data points, respectively. The Gaussian fits are denoted by the solid lines.

through eqs 3 and 4, then the achievement requires five photons. The proposed mechanism is against the measurements of laser power dependence yielding a slope about 3, which implies that the ionization step of iodine is saturated.

The available energy E_{avl} for the dissociation process may be calculated by

$$E_{avl} = E_{h\upsilon} - D_0 - E_{el} + E_{int} \qquad (5)$$

where $E_{h\upsilon}$ is the photon energy; D_0 is the C−I bond dissociation energy evaluated to be 2.353 eV for C_2H_5I;[34] E_{el} is the electronic energy level of the iodine atom, zero for I and 7603 cm^{-1} for I*; and E_{int} is the internal energy of the parent molecule, which

Photodissociation Dynamics of Ethyl Iodide

J. Phys. Chem. A, Vol. 113, No. 1, 2009 **37**

TABLE 1: Summary of Dynamical Parameters in the Photodissociation of C_2H_5I

wavelength (nm)	state	E_{avl} (kJ/mol)	E_t (kJ/mol)	f_t	β	$\Phi(I^*)$	P_{cc}
294.1	I*	88.6	65.6	0.74	2.0	0.51 ± 0.10	0.45 ± 0.10
298.2	I	173.9	111.6	0.64	1.6 ± 0.1		
304.0	I*	75.2	56.8	0.76	2.0	0.20	0.81
303.7	I	166.4	107	0.64	1.7 ± 0.1		
305.6	I*	73.6	55.5	0.75	2.0	0.20	0.78
304.7	I	165.1	105.3	0.64	1.7 ± 0.1		
306.6	I*	72.1	51.2	0.71	2.0	0.21	0.79
307.6	I	161.5	96.5	0.61	1.9 ± 0.1		

is considered as zero in a supersonic molecular beam. The center-of-mass translational energy carried by the dissociating species can be evaluated from the velocity of an individual fragment. The fraction of the translational energy release, f_T, defined as a ratio of the average translational energy $\langle E_T \rangle$ to the available energy E_{avl}, is then estimated to be 0.61−0.64 and 0.71−0.76 for the I and I* channels, respectively, indicating that the I channel may carry more internal energy in the C_2H_5 moiety. This fact is also reflected in a wider speed distribution of the I fragment (Figures 1 and 2), which suggests that the accompanied C_2H_5 be in hotter internal states than the other channel leading to I* + C_2H_5. The $f_T(I)$ and $f_T(I^*)$ values are consistent with 0.68 and 0.72, respectively, obtained at 304 nm,[25] and comparable with 0.62−0.65 and 0.72−0.75 obtained at the shorter photolyzing wavelengths from 245 to 283 nm.[21,31] They are also comparable with those obtained in CH_3I. But $f_T(I)$ and $f_T(I^*)$ may be reduced to 0.52−0.55 and 0.55−0.59, respectively, at either 266 or 304 nm in ICH_2CN in which an electron-withdrawing group is substituted.[35] More energy is deposited in the internal states of CH_2CN.

The relative quantum yields Φ of the I and I* channels may be evaluated by

$$\Phi(I^*) = \frac{N(I^*)}{N(I) + N(I^*)} = k\frac{S(I^*)}{S(I) + S(I^*)} \quad (6)$$

and

$$\Phi(I) = 1 - \Phi(I^*) \quad (7)$$

Here, $N(I^*)$ and $N(I)$ are the numbers of I* and I fragments; $S(I^*)$ and $S(I)$ are the REMPI signals that are measured individually. The factor k, which relates the obtained iodine ion signal to its state population, can be evaluated by performing a calibration experiment of I_2 photolysis under the same conditions. The factor k was determined to be 5.9, 0.25, 2.0, and 0.67 at the photolyzing wavelengths of 294.05/298.23, 303.69/304.03, 304.68/305.57, and 306.63/307.64 nm, respectively, by assuming identical intensities of the I and I* fragments at each pair of wavelengths. The $\Phi(I^*)$ value thus obtained decreases from 0.51 to 0.2 with increasing the photolyzing wavelength, and then remains almost at 0.2. Their results are listed in Table 1.
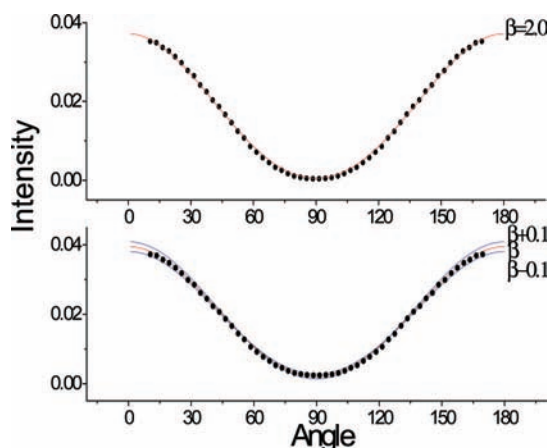
In a photodissociation process, angular distribution $I(\theta)$ of the fragment is obtained by integrating the reconstructed three-dimensional spatial distribution over a proper range of speed at each angle. It may be characterized by an anisotropy parameter, β, according to the following equation,[36,37]

$$I(\theta) = (4\pi)^{-1}[1 + \beta P_2(\cos\theta)] \quad (8)$$

Here, $P_2(\cos\theta)$ is the second-order Legendre polynomial, and θ is the angle between the laser polarization direction and the recoil velocity of fragments. The β value can be determined by least-squares fit to the angular distribution. Figure 3 gives an

example for the $\beta(I)$ and $\beta(I^*)$ fits at the wavelengths of 303.7/304.0 nm. In this manner, the β values are obtained at various wavelengths. The dynamical properties at the wavelengths studied are all listed in Table 1. It should be noted that the obtained anisotropy parameters may be somehow interfered with by the laser-induced molecular alignment effect, when a single laser radiation is employed for the role of both photolysis and ionization. Dynamic alignment of CH_3I was previously reported by nanosecond laser pulses at intensities $<10^{12}$ W/cm² and by picosecond laser pulses at higher intensities of $10^{14}-10^{15}$ W/cm².[38-40] The use of a laser field of moderate intensity can result in molecular alignment due to the coupling of the laser field with the induced dipole moment. Once it happens, the angular distribution of subsequent atomic fragments may be characterized by a product of the orientational probability distribution of the parent molecule and the recoil distribution given in eq 8 for the fast axial photodissociation.[41] In this work, the maximum energy intensity is controlled as small as $<5 \times 10^9$ W/cm². Thus, the caused molecular and atomic alignment effect should be minimized.

B. Nonadiabatic Transition. The A-band of ethyl iodide is mainly contributed by $^3Q_0$ covering 81% of the total absorption cross section with the maximum at 38820 cm⁻¹ and full width at half-maximum (fwhm) of 5060 cm⁻¹. The other two small components are $^3Q_1$ sharing 9% with the maximum at 36500 cm⁻¹ and fwhm 4060 cm⁻¹, and $^1Q_1$ sharing 10% with the maximum at 40275 cm⁻¹ and fwhm 3530 cm⁻¹.[42] Thus, the $^3Q_0$ and $^3Q_1$ states dominate over the excitation wavelengths studied. The $\beta(I^*)$ values over the full wavelengths are obtained to be 2.0 (Table 1), suggesting that the I* product should be contributed from the $^3Q_0$ state alone. Apart from the direct excitation of $^3Q_1$, the I channel with a positive $\beta(I)$ indicates

Figure 3. β determination by the fit of angular distribution in the photodissociation of C_2H_5I. (upper) $\beta = 2.0$ at 304.0 nm for the I*-product channel, and (lower) $\beta = 1.7 \pm 0.1$ at 303.7 nm for the I-product channel.
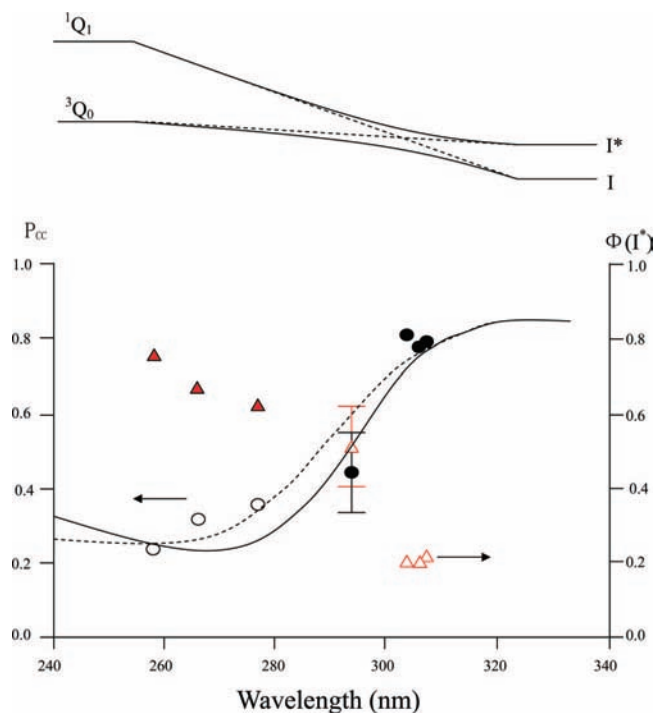
Figure 4. Nonadiabatic transition probability and quantum yield of the I* channel as a function of the dissociation wavelength. (○) and (▲) denote the data adopted from ref 31, and (●) and (△) denote the present work. The solid curve is from the experimental findings in CH$_3$I (ref 12), and the dashed line is expected by the Landau−Zener model.

that a significant contribution comes from the $^3Q_0 \rightarrow {}^1Q_1$ nonadiabatic transition. The direct contribution in the I channel is considered to have a perpendicular character ($\beta = -1$), whereas the nonadiabatic contribution remains the same anisotropy as the I* channel. Therefore, the $\beta(I)$ value may be resolved into the relative contributions of the parallel and perpendicular components by the formula,

$$\beta(I) = a\beta_{\parallel} + b\beta_{\perp} = a\beta(I^*) + b(-1) \qquad (9)$$

where a and b, having a sum equal to unity, denote the fractions of nonadiabatic and direct-excitation contributions in the I-product channel. The curve crossing probability, P_{cc}, between the $^3Q_0$ and $^1Q_1$ states can be evaluated by the following equation,[12,31]

$$P_{cc} = \frac{a(1 - \Phi(I^*))}{\Phi(I^*) + a(1 - \Phi(I^*))} \qquad (10)$$

Given the measures of $\beta(I)$, $\beta(I^*)$, and $\Phi(I^*)$, P_{cc} may be determined to be 0.45 ± 0.10, 0.81, 0.78, and 0.79 at 294.05/298.23, 303.69/304.03, 304.68/305.57, 306.63/307.64 nm, respectively. The results are also listed in Table 1.

Figure 4 shows the nonadiabatic transition probability as a function of the excitation wavelength from 258 to 308 nm, in comparison with those obtained in the CH$_3$I photodissociation.[12] The data at <280 nm are referred to the previous work.[31] The wavelength dependence of $\Phi(I^*)$ is also shown in Figure 4. Note that the datum at 294.05/298.23 nm carries a large uncertainty, because the selected wavelengths in this pair are far from each other. In the calibration experiments in which I$_2$ is dissociated individually at 294.1 and 298.2 nm, we neglect the wavelength dependence of photodissociation cross section of I$_2$. That is, the resulting I and I* intensities are assumed to be the same at these two wavelengths in determining $\Phi(I^*)$ and

the subsequent P_{cc}. However, this assumption is skeptical at such far separated wavelengths and the datum obtained at 294.05/298.23 nm is less reliable.

In the photodissociation of CH$_3$I, the location of the $^3Q_0 - {}^1Q_1$ curve crossing has been predicted experimentally and theoretically. As photodissociation occurs in a closer distance to the Landau−Zener type crossing point, the nonadiabatic transition probability is expected to increase. On the basis of a sharp increase in the perpendicular component for the emission spectra, Butler and co-workers suggested that the curve crossing should lie at 2.35 Å along the C−I bond coordinate with the excitation wavelength between 298.5 and 303.0 nm,[43] which agrees with the calculated result of 298.2 nm by Alekseyev et al.,[16] but different from the prediction of 324.2 nm by Ajitha et al.[44] Alekseyev et al. recently obtained the $^3Q_0 - {}^1Q_1$ crossing at the C−I distance of 2.37 Å and the umbrella angle of 114° in the calculations of two-dimensional potential energy surfaces.[16] The results are consistent with the previous theoretical predictions of 2.38 Å and 114° as well as 2.34 Å and 114.3°.[14,44]

The curve crossing may be alternatively estimated by evoking a modified one-dimensional Landau−Zener theory as expressed by[22,45]

$$\Phi(I^*) = \exp\left(-\frac{\rho}{2(E_{h\nu} - E_{cc})^{1/2}}\right) \qquad (11)$$

where ρ denotes the modified Landau−Zener parameter which remains constant for the same system, $E_{h\nu}$ is the photodissociation energy, and E_{cc} is the energy of the curve crossing point. Given the quantum yields of I* at different photodissociation energies, E_{cc} may be readily estimated. In terms of $\Phi(I^*)$ obtained at 266 and 304 nm, Li et al.[22] estimated the potential energy at the curve crossing point to be 32790 cm^{-1}, equivalent to an excitation wavelength of 305.0 nm which is slightly longer than those obtained above.[16,43]

Our results in Figure 4 reveal that the nonadiabatic transition probability increases gradually in the early stage and then rises up dramatically with the increased wavelength. The abrupt increase of the perpendicular character suggests that the conical intersection between the $^3Q_0$ and $^1Q_1$ states may be around 304 nm.[43] Given four $\Phi(I^*)$ data obtained at 266.5/266.6, 277.4/277.9, 303.7/304.0, and 304.7/305.6 nm that are substituted in eq 11, the energy at the curve crossing point is estimated to be 32602−32475 cm^{-1}, corresponding to the excitation wavelength of 306.7−307.9 nm. The reliable curve crossing point is thus considered to be between 304 and 306.7 nm. When the dissociation wavelength is tuned to pass the conical intersection, P_{cc} drops only by <4%, suggesting that these two curves may cross almost parallel in the exit channel. Unfortunately, no significant signals of the I/I* pairs may be obtained when the photolyzing wavelength exceeds 308 nm. On the other hand, $\Phi(I^*)$ decreases with the wavelength and then rises slightly after passing the conical intersection. Increasing the $^3Q_0 \rightarrow {}^1Q_1$ nonadiabatic transition should bring about the decrease of $\Phi(I^*)$. As shown in Figure 4, the nonadiabatic transition probabilities in this work behave similarly as those observed in the case of CH$_3$I but are slightly enhanced by the branched ethyl group at a given photolyzing wavelength. The P_{cc} value is expected to increase as the α-branched alkyl group becomes massive and the subsequent moving speed through the Landau−Zener crossing region becomes slower.

The vibrational spectra of the alkyl iodide cations are dominated by a long progression of CI stretch mode, followed by a CCI (or HCI in methyl iodide) bending mode (fundamental and combination).[6,18−20,46] These two modes are associated with

Photodissociation Dynamics of Ethyl Iodide

J. Phys. Chem. A, Vol. 113, No. 1, 2009 **39**

the earlier dissociation behavior and disappear after breaking apart of the cations. The photodissociation process is thus anticipated to involve coupling primarily between the CI internal coordinate and the bending mode. The nonadiabatic transition is substantially affected by the coupling strength between crossing curves. The one-dimensional Landau−Zener theory indicates that a stronger coupling between two crossing states may result in a larger adiabatic curve splitting and the subsequent nonadiabatic transition probability, P_{cc}. Although the photodissociation of alkyl iodides involves multidimensional character, a stronger coupling strength may analogously result in a larger P_{cc}. As the α-branched alkyl group becomes heavier, the contribution from the bending fundamental and combination modes becomes larger relative to the CI stretch progression.[6,18,46] Accordingly, the umbrella mode of CH_3 in the photodissociation of CH_3I at 266 and 304 nm is found to reach $v_2 = 4$ in the I-product channel,[22] whereas the v_2 mode of C_2H_5 can be extended to >11 and >8 in the photodissociation of C_2H_5I at 279.7 and 304 nm, respectively.[47] In this sense, the C_2H_5I photodissociation should tend to have a larger nonadiabatic transition rate that is, however, not clear enough in our previous work.[31]

IV. Conclusion

The photodissociation dynamics of ethyl iodide over the wavelength range of 294−308 nm has been investigated, in supplement to the work obtained similarly with shorter dissociation wavelengths.[31] As expected, the I* channel, originating from the $^3Q_0$ state alone, is accompanied by colder internal states of C_2H_5, whereas the I channel, contributed by direct excitation and nonadiabatic transition, is with a hotter C_2H_5. The curve crossing probability rises rapidly around the conical intersection but remains almost constant after passing through the curve crossing. The $^1Q_1$ and $^3Q_0$ states in the exit region are thus expected to cross almost parallel along the dissociation coordinate. As compared to the photodissociation of CH_3I at the same photolyzing wavelength, the nonadiabatic transition probabilities are slightly enhanced by an ethyl-substituted group.

References and Notes

(1) Mulliken, R. S. *J. Chem. Phys.* **1940**, *8*, 382.
(2) Guo, H.; Schatz, G. C. *J. Chem. Phys.* **1990**, *93*, 393.
(3) Johnson, B. R.; Kittrell, C.; Kelly, P. B.; Kinsey, J. L. *J. Phys. Chem.* **1996**, *100*, 7743.
(4) Jung, Y. J.; Kim, Y. S.; Kang, W. K.; Jung, K. H. *J. Chem. Phys.* **1997**, *107*, 7187.
(5) Zhong, D.; Zewail, A. H. *J. Phys. Chem. A* **1998**, *102*, 4031.
(6) Samartzis, P. C.; Bakker, B. L.; Parker, D. H.; Kitsopoulos, T. N. *J. Phys. Chem. A* **1999**, *103*, 6106.
(7) Wu, G.; Jiang, B.; Ran, Q.; Zhang, J.; Harich, S. A.; Yang, X. *J. Chem. Phys.* **2004**, *120*, 2193.
(8) Eppink, A. T. J. B.; Parker, D. H. *J. Chem. Phys.* **1999**, *110*, 832.

(9) Xu, H.; Guo, Y.; Liu, S.; Ma, X.; Dai, D.; Sha, G. *J. Chem. Phys.* **2002**, *117*, 5722.
(10) Rijs, A. M.; Janssen, M. H. M.; Chrysostom, E. T. H.; Hayden, C. C. *Phys. Rev. Lett.* **2004**, *92*, 123002.
(11) Hu, C.; Pei, S.; Chen, Y. L.; Liu, K. *J. Phys. Chem. A* **2007**, *111*, 6813.
(12) Eppink, A. T. J. B.; Parker, D. H. *J. Chem. Phys.* **1998**, *109*, 4758.
(13) van Veen, G. N. A.; Baller, T.; de Vires, A. E.; van Veen, N. J. A. *Chem. Phys.* **1984**, *87*, 405.
(14) Amatatsu, Y.; Yabushita, S.; Morokuma, K. *J. Chem. Phys.* **1996**, *104*, 9783.
(15) Talukdar, R. K.; Vaghjiani, G. L.; Ravishankara, A. R. *J. Chem. Phys.* **1992**, *96*, 8194.
(16) Alekseyev, A. B.; Liebermann, H.-P.; Buenker, R. J.; Yurchenko, S. N. *J. Chem. Phys.* **2007**, *126*, 234102.
(17) de Nalda, R.; Lzquierdo, J. G.; Dura, J.; Banares, L. *J. Chem. Phys.* **2007**, *126*, 021101.
(18) Philips, D. L.; Lawrence, B. A.; J, J.; Valentini, *J. Phys. Chem.* **1991**, *95*, 9085.
(19) Philips, D. L.; Myers, A. B.; Valentini, J. J. *J. Phys. Chem.* **1992**, *96*, 2039.
(20) Philips, D. L.; Meyers, A. B. *J. Chem. Phys.* **1991**, *95*, 226.
(21) Paterson, C.; Codwin, F. G.; Gorry, P. A. *Mol. Phys.* **1987**, *60*, 729.
(22) Li, G.; Shin, Y. K.; Hwang, H. J. *J. Phys. Chem. A* **2005**, *109*, 9226.
(23) Uma, S.; Das, P. K. *J. Chem. Phys.* **1996**, *104*, 4470.
(24) Kim, Y. S.; Kang, W. K.; Kim, D. C.; Jung, K. H. *J. Phys. Chem. A* **1997**, *101*, 7576.
(25) Kang, W. K.; Jung, K. W.; Kim, D. C.; Jung, K. H.; Im, H. S. *Chem. Phys.* **1995**, *196*, 363.
(26) North, S. W.; Sears, T. J.; Hall, G. E.; Suzuki, T. *Chem. Phys.* **1996**, *211*, 515.
(27) Rattigan, O. V.; Shallcross, D. E.; Cox, R. A. *J. Chem. Soc., Faraday Trans.* **1997**, *93*, 2839.
(28) Roehl, C. M.; Burkholder, J. B.; Moortgat, G. K.; Ravishankara, A. R.; Crutzen, P. J. *J. Geophys. Res.* **1997**, *102*, 12819.
(29) Brewer, P.; Das, P.; Ondrey, G. S. *J. Chem. Phys.* **1983**, *79*, 720.
(30) Godwin, F. G.; Gorry, P. A.; Hughes, P. M. *Chem. Phys. Lett.* **1987**, *135*, 163.
(31) Tang, Y.; Lee, W. B.; Hu, Z.; Zhang, B.; Lin, K. C. *J. Chem. Phys.* **2007**, *126*, 064302.
(32) Tang, Y.; Lee, W. B.; Zhang, B.; Lin, K. C. *J. Phys. Chem. A.* **2008**, *112*, 1421.
(33) Hu, Z.; Lee, W. B.; Zhang, X. P.; Wei, P. Y.; Lin, K. C. *ChemPhysChem.* **2008**, *9*, 422.
(34) Fan, H.; Pratt, S. T. *J. Chem. Phys.* **2005**, *123*, 204301.
(35) Lee, K. S.; Lim, J. S.; Ahn, D. S.; Choi, K. W.; Kim, S. K.; Choi, Y. S. *J. Chem. Phys.* **2006**, *124*, 124307.
(36) Zare, R. N.; Herschbach, D. R. *Proc. IEEE.* **1963**, *51*, 173.
(37) Zare, R. N. *Mol. Photochem.* **1972**, *4*, 1.
(38) Larsen, J. J.; Sakai, H.; Safvan, C. P.; Wendt-Larsen, I.; Stapelfeldt, H. *J. Chem. Phys.* **1999**, *111*, 7774.
(39) Sugita, A.; Mashino, M.; Kawasaki, M.; Matsumi, Y.; Gordon, R. J.; Bersohn, R. *J. Chem. Phys.* **2000**, *112*, 2164.
(40) Kaziannis, S.; Kosmidis, S. C. *Chem. Phys. Lett.* **2005**, *401*, 115.
(41) Janssen, M. H. M.; Mastenbroek, J. W. G.; Stolte, S. *J. Phys. Chem. A* **1997**, *101*, 7605.
(42) Gedanken, A. *Chem. Phys. Lett.* **1987**, *137*, 462.
(43) Lao, K. Q.; Person, M. D.; Xayariboun, P.; Butler, L. J. *J. Chem. Phys.* **1990**, *92*, 823.
(44) Ajitha, D.; Wierzbowska, M.; Lindh, R.; Malmqvist, P. A. *J. Chem. Phys.* **2004**, *121*, 5761.
(45) Codwin, F. G.; Paterson, C.; Gorry, P. A. *Mol. Phys.* **1987**, *61*, 827.
(46) Knoblauch, N.; Strobel, A.; Fischer, I.; Bondybey, V. E. *J. Chem. Phys.* **1995**, *103*, 5417.
(47) Bi, W. B.; Xu, X. L.; Huang, J. G.; Xiao, D. Q.; Zhu, Q. H. *Sci. China Ser. B-Chem.* **2007**, *50*, 476.